GABA, glucose and insulin orchestrate CD4$^+$ T cells effector functions

Jin[1]# Z, Hammoud[1]# H, Bhandage[1] AK, Korol[1] SV, Trujeque-Ramos[1] O, Koreli[1] S., Chowdhury[1] AI, Sandbaumhüter[2] FA, Jansson[2] ET, Andrén[2] PE, Bergsten[1] P, Kamali-Moghaddam[3] M, Birnir* B

[1] Department of Medical Cell Biology, Uppsala University, Uppsala, Sweden

[2] Department of Pharmaceutical Biosciences, Uppsala University, Uppsala, Sweden.

[3] Department of Immunology, Genetics and Pathology, Science for Life Laboratory, Uppsala University, Uppsala, Sweden

 # Contributed equally

*** Correspondence**

Prof Bryndis Birnir

Department of Medical Cell Biology

Uppsala University

Uppsala, 75124, Sweden

Email: bryndis.birnir@mcb.uu.se

Tel: +46765620243

Summary

Metabolic programs of immune cells are closely linked to their effector functions[1], where physiological molecules provide environmental cues and guidance[2-5]. Exactly how it happens is still being unraveled. Insulin maintains normal blood glucose levels[6] and glucose is the main source of energy and a precursor for many biomolecules in T cells[7,8], whereas γ-aminobutyric acid (GABA), best known as a neurotransmitter, is increasingly recognized as a regulatory molecule in the immune system[4,9]. Here, we demonstrate that GABA-mediated reduction of metabolic activity and release of inflammatory molecules, including IFNγ and IL-10, was abolished in human $CD4^+$ T cells, when the glucose concentration was elevated above normal levels. In a glucose concentration-dependent manner, insulin enhanced the $GABA_A$ receptors activated currents and GABA-dependent Ca^{2+} influx. GABA decreased, whereas insulin maintained glycolysis but in a SGLT (Na^+-glucose transporter)-dependent manner, revealing expression of SGLTs in activated $CD4^+$ T cells. The SGLTs antagonist phlorizin, alone or together with GABA, restored the inhibition of IFNγ and IL-10 release in presence of high glucose. This study exposes concerted effects of GABA, glucose and insulin on $CD4^+$ T cells metabolic activity and release of inflammatory molecules, and identifies a role for SGLTs in $CD4^+$ T cells function.

43 **Main**

44 **GABA inhibition is affected by glucose**

45 Physiological blood glucose concentration 2h after a meal, is normally maintained
46 around 5.6 mM in healthy individuals, while it is higher in diseases such as diabetes (> 7 mM)
47 or Covid-19[10]. Metabolic activity of T cells is closely related to their rate of proliferation. We
48 examined effects of four glucose concentrations on the GABA inhibition of metabolic activity
49 of $CD4^+$ T cells (N=35–53 human donors; Figure 1a; Extended Data Table 1; Extended Data
50 Figure 1). At glucose concentrations higher than the physiological level (10 mM and 16.7 mM),
51 the inhibition by GABA was abolished (Figure 1a; Extended Data Figure 2a). When the GABA
52 responses were compiled based on low-normal (2.8 mM, 5.6 mM) or high (10 mM, 16.7 mM)
53 glucose concentrations a clear shift was observed for GABA's inhibitory response. At the level
54 0.9 or lower metabolic activity (Figure 1b left panel), cells from 74% of the donors were
55 inhibited by GABA in the low-normal glucose group. The metabolic activity of cells from these
56 same donors were not inhibited at the higher glucose concentrations (Figure 1b right panel;
57 Extended Data Figure 2b). Intrigued by these results, we sought whether glucose affected
58 other immunological functions regulated by GABA. Since glycolysis feeds substrates into
59 anabolic metabolism, we studied if glucose modulated the GABA-inhibition of release of
60 biomolecules from $CD4^+$ T cells from the same donors (N=18) cultured in low-normal or high
61 glucose. In each sample, 92 inflammation-related biomolecules commonly associated with
62 inflammation were measured using Olink Target Inflammation protein panel, which is based
63 on the multiplex proximity extension assay (PEA) technology. A total of 59 different proteins
64 were detected. Similar to the results from the metabolic activity, the GABA-inhibition of
65 proteins released from $CD4^+$ T cells was glucose concentration-dependent (Figure 1c). The
66 GABA inhibition was optimal at the physiological glucose concentration (5.6 mM), where

67 GABA decreased the release of 37 proteins. In contrast, GABA did not affect release of
68 proteins in neither 10 mM nor 16.7 mM glucose (Figure 1c). ELISA confirmed the PEA results
69 for two cytokines; interferon gamma (IFNγ), the principal cytokine of $CD4^+$ T helper1 cells and
70 interleukin-10 (IL-10), the principal cytokine for $CD4^+$ T helper2 and T regulatory cells (Figure
71 1d, e). In contrast, in absence of GABA, increasing the glucose concentration alone enhanced
72 release of IFNγ (Extended Data Figure 2c) but not IL-10 (Extended Data Figure 2d). Thus, GABA-
73 dependent regulation of $CD4^+$ T cells is linked to the extracellular glucose concentration.

74 Insulin is normally associated with glucose homeostasis. However, at least in excitable
75 cells, insulin is also a regulator of GABA signaling[11-13]. The insulin receptor is not expressed in
76 resting T cells but is prominent at 48 h post-activation[14].GABA activates two types of receptors
77 in cell membranes; the $GABA_A$ receptor ($GABA_AR$), a pentameric chloride ion channel, that
78 opens when GABA binds to the receptor and the $GABA_B$ receptor ($GABA_BR$), a G-protein
79 coupled receptor, that is formed as a dimer**.** To-date, only one of the two $GABA_B$ isoforms
80 required for function has been detected in immune cells, whereas several $GABA_A$ receptor
81 subunits are identified in T cells[4,15]. The $GABA_AR$ ρ2 (*GABRR2*) is a highly expressed subunit in
82 peripheral blood mononuclear cells[15]. Irrespective of glucose concentration, activation of
83 $CD4^+$ T cells decreased the expression of the *GABRR2* transcript relative to resting cells,
84 whereas insulin increased the expression of the *GABRR2* (Figure 1f). The protein was detected
85 by a GABRR2 specific antibody by fluorescent labelling the $CD4^+$ T cells (Figure 1g).

86 **Insulin enhances the GABA-activated currents**

87 We measured the GABA-activated $GABA_AR$ currents in intact activated $CD4^+$ cells using
88 perforated patch-clamp electrophysiology. Since the intracellular environment is unchanged,
89 intracellular signaling that may take place is expected to function normally. The 500 nM GABA-
90 activated $GABA_AR$-mediated currents were blocked by the $GABA_AR$ antagonist picrotoxin and

91 enhanced by insulin at 5.6 mM glucose (Figure 2a). The apparent GABA affinity (EC_{50}) for
92 $GABA_AR$ was similar in 5.6 mM and 16.7 mM glucose, 0.7 nM and 0.9 nM GABA, respectively.
93 Insulin then shifted the EC_{50} values more than 10-fold, to 0.04 nM and 0.06 nM GABA (Figure
94 2b, c). The $GABA_AR$ agonists muscimol and TACA evoked currents similar to GABA (Figure 2d).
95 The currents reversed at −37 mV (Extended Data Figure 3a), close to the calculated reversal
96 potential for chloride (E_{Cl} = −39 mV). By regulating the membrane potential these very
97 sensitive $GABA_AR$ channels may affect activity of other ion channels or flow of ions across the
98 cell membrane[16].

99 **Insulin enhances GABA-activated Ca^{2+} entry**

100 The cytoplasmic concentration of Ca^{2+} ions is tightly regulated in T cells but can be
101 increased by release from intracellular stores or by entry through plasma membrane Ca^{2+} ion
102 channels[17]. A representative live cell-Ca^{2+} recording trace measured from activated $CD4^+$ T
103 cells (Figure 2e) showed that acute GABA (500 nM) application induced transient calcium
104 signal, which was, in fact, influx of extracellular calcium and not due to release from
105 intracellular stores as no signal could be detected in absence of extracellular calcium (Figure
106 2e, left panel). Analyzed live cell-Ca^{2+} recording data from four donors is shown in Figure 2e,
107 right panel. Transient change in glucose from 5.5 to 16.7 mM did not alter the 500 nM GABA-
108 activated Ca^{2+} response (Extended Data Figure 3b). Insulin incubation of cells enhanced the
109 GABA induced Ca^{2+} signals in 5.5 mM but not in 16.7 mM glucose (Figure 2f), whereas no
110 differences were observed for baseline Ca^{2+} levels in cells with or without insulin incubation
111 (Extended Data Figure 3c). The GABA-activated Ca^{2+} signal was blocked by the $GABA_AR$
112 antagonist picrotoxin (Figure 2g), while no effect was observed by the $GABA_BR$ antagonist,
113 CGP52432 (Extended Data Figure 3d). This prompted us to examine dose-response
114 relationship between GABA and the Ca^{2+} signals in cells with or without insulin incubation

115 (Figure 2h, i, j; Extended Data Figure 3e). Representative time-lapse recording of a $CD4^+$ T cell,
116 16.7 mM glucose, with insulin, demonstrates that raising GABA concentrations induced
117 increasing Ca^{2+} signals (Figure 2h). Insulin incubation of the cells lowered the EC_{50} values of
118 the GABA-activated Ca^{2+} signals. The apparent GABA affinity of the Ca^{2+} signal was 55 nM and
119 113 nM GABA in 5.5 mM and 16.7 mM glucose, and shifted more than 1000-fold to 0.009 nM
120 and 0.09 nM GABA with insulin, respectively (Figure 2i, j). The Ca^{2+} response to $GABA_AR$
121 agonists, muscimol and TACA, and antagonists, TPMPA and picrotoxin, further confirmed the
122 $GABA_AR$ connection in the evoked Ca^{2+} signal (Figure 2k, l, m). Ca^{2+} release-activated
123 Ca^{2+} (CRAC) channels mediate store operated calcium entry (SOCE) in T cells that is central to
124 the Ca^{2+} homeostasis and cytoplasmic Ca^{2+} levels[17]. The GABA-activated Ca^{2+} signal was
125 inhibited by 1 µM YM48583 (Figure 2n), an antagonist of SOCE, revealing the Ca^{2+} ion channel
126 participating in the cascade. The tight scaling of the Ca^{2+} signal from $GABA_AR$ activation to Ca^{2+}
127 entry and the sensitization by insulin identifies a specific, focused mechanism regulating Ca^{2+}
128 signaling in $CD4^+$ T cells.

129 Insulin is known to regulate intracellular signaling and gene expression, whereas less
130 is known about effects of GABA. However, out of the nine examined genes encoding
131 transcription factors or kinases, only *NFATC2* (nuclear factor of activated T cells) was
132 significantly reduced by GABA at 5.6 mM glucose (Extended Data Table 2). NFATs proteins are
133 activated by increased Ca^{2+} in the cytoplasm and translocate to the nucleus, where they
134 regulate transcription of many proteins including inflammatory molecules[18].

135 **GABA regulation of glycolysis is glucose-dependent**

136 That GABA regulated expression of signaling pathways and proteins was revealed by
137 mass spectrometry (MS) of activated $CD4^+$ T cells cultured in the presence or absence of GABA
138 (Figure 3a, Extended Data Table 3). Hexokinase 1 (HK1), the first enzyme in the glycolytic

139 pathway, was significantly down-regulated by GABA in both 5.6 mM and 16.7 mM glucose
140 (Figure 3b). HK activity was negligible under resting conditions but increased about 60 times
141 in activated $CD4^+$ T cells in both 5.6 mM and 16.7 mM glucose. Intriguingly, GABA decreased
142 the HK activity only at 5.6 mM glucose and insulin had no further effect (Figure 3c). T cells
143 switch to aerobic glycolysis upon activation as their predominant way to generate adenosine
144 5´-triphosphate (ATP) and accumulate biomass[19,20], the so-called Warburg effect. It results in
145 glucose-derived pyruvate being converted to lactate that can be detected by measuring
146 extracellular acidification rate (ECAR)[21]. Since HK is the gate-keeper for the glycolytic pathway,
147 we examined if glucose, GABA or insulin modulated glycolysis. Representative ECAR traces
148 and average values for activated $CD4^+$ T cells at 5.6 mM and 16.7 mM glucose in the presence
149 or absence of GABA and insulin are shown in Figure 3d and e. GABA but not insulin inhibited
150 glycolysis and glycolytic capacity but only in 5.6 mM glucose. No effect of GABA at higher
151 glucose suggested the possibility that either the intracellular glucose might affect the GABA
152 inhibition of glycolysis or there were other competing mechanisms at work.

153 **SGLT2 in $CD4^+$ T cells**

154 Facilitated glucose transport is the main route for glucose entry into activated T cells[3].
155 We confirmed the dominance of the facilitated transport by examining the effects of an
156 antagonist of GLUTs, WZB117 (WZB), on the cellular metabolic activity of activated $CD4^+$ T cells
157 (Figure 4a), whereas phlorizin, an antagonist of Na^+-dependent glucose transport (SGLT1 and
158 SGLT2)[22], had no effect at either glucose concentration (Figure 4a). Nevertheless, *SLC5A2*, the
159 gene encoding SGLT2, was detected by RNAseq analysis from activated $CD4^+$ T cells (Figure
160 4b) and the protein was also expressed (Figure 4c, d). In presence of phlorizin or empagliflozin,
161 a more specific SGLT2 antagonist and a prescription medicine in type 2 diabetes, a significant
162 reduction in glucose uptake was observed in insulin incubated cells (Figure 4e). Phlorizin alone

163 reduced glycolysis and glycolytic capacity at both 5.6 mM and 16.7 mM glucose (Figure 4f),
164 whereas insulin reduced or abolished the inhibition by phlorizin (Figure 4f). Since phlorizin
165 reduced glycolysis, it could be expected to reduce synthesis of biomolecules such as IFNγ and
166 IL-10, similar effects to what we observed for GABA (see Figure 1c, d, e). Indeed, phlorizin
167 reduced release of IFNγ and IL-10 at both 5.6 mM and 16.7 mM glucose even in the presence
168 of insulin (Figure 4g, h) with the exception of IFNγ at 16.7 mM glucose with insulin, where only
169 phlorizin together with GABA reduced IFNγ release, approximately 50%. In general, there was
170 a trend for GABA to enhance the phlorizin reduction of release of IFNγ and IL-10. The results
171 demonstrate functional Na^+-dependent glucose carriers in $CD4^+$ T cells and identify their
172 relevance for production of cytokines.

173 **Discussion**

174 T cells modulate their metabolism to adapt to different environments[1,19,20]. When
175 $CD4^+$ T cells are activated, their metabolic activity is altered to meet the demands of cell
176 growth, proliferation and effector functions. Here we revealed that GABA, glucose and insulin
177 together orchestrate functions of $CD4^+$ T cell, to coordinate and to set the activity level of
178 distinct cellular pathways linked to glucose metabolism and that are central for
179 immunometabolism and T cells effector functions (Extended Figure 4).

180 Proliferating T cells shift their metabolic phenotype to aerobic glycolysis at the expense
181 of mitochondrial oxidative phosphorylation[19,23]. Although this switch is inefficient in terms of
182 generating ATP, it confers advantage for the biosynthetic pathways that branch out from
183 glycolysis[19,20]. GABA decreased cellular metabolic activity and release of proteins in a glucose
184 concentration-dependent manner. Insulin shifted the $GABA_AR$ signaling by making it
185 supersensitive to GABA and consequently enhanced Ca^{2+} entry through CRAC channels, an

186 elegant way of modulating intracellular Ca^{2+} levels and intracellular processes affecting T cells
187 effector functions.

188 It was surprising that extracellular glucose modulated the GABA inhibition to regulate
189 effector functions of T cells. Although glucose transport in $CD4^+$ T cells is mainly mediated by
190 facilitated glucose transporters, the present results identified significant Na^+-dependent
191 glucose transport relevant for the effector functions. HK is the first enzyme in the glycolytic
192 pathway and by converting glucose to glucose-6-phosphate (G-6-P), traps glucose within the
193 cell[7]. Human HK has normally maximum activity in 5 mM glucose in the presence of natural
194 inhibitors, such as G-6-P[24], but HK activity is increased at glucose concentrations > 5 mM[24].
195 This is in line with our results, where GABA only succeeded decreasing HK enzymatic activity
196 in 5.6 mM glucose. Na^+-dependent glucose transport drives glucose into cells even at high
197 intracellular glucose concentrations[22]. Glucose competes with G-6-P for the binding site on
198 HK[24], decreasing the inhibition of HK[24], which results in increased substrate availability for
199 biosynthesis[8]. Aerobic glycolysis directly regulates synthesis of IFNγ[25] by engaging
200 glyceraldehyde-3-phosphate dehydrogenase (GDPDH) and, thereby, relieving its inhibition of
201 IFNγ mRNA translation. In concordance, activated $CD4^+$ cells secreted more IFNγ in high
202 glucose. GABA promoted a glycolytic switch to lower values for both glycolysis and the
203 glycolytic capacity in 5.6 mM glucose that was gone in 16.7 mM glucose, whereas phlorizin
204 was effective inhibitor at both glucose concentrations and, in particular, in the absence of
205 insulin. Discovering that $GABA_AR$ activation together with SGLT2 inhibition can dramatically
206 reduce the levels of IFNγ and IL-10, at both normal and high glucose concentrations, has
207 implications for regulation of inflammation, as availability of biosynthetic intermediates-
208 production fuels effector signaling molecules and functions[8].

209 $GABA_A$Rs are widespread in the brain and are present in many other tissues[26] but
210 $GABA_A$Rs containing GABRR2 (ρ2 subunit) are rare outside the immune system, with the
211 exception of the retina[27]. $GABA_A$R-ρ2 might be a valuable and a rather specific drug target[28].
212 SGLT2 inhibitors such as empagliflozin, are already in clinical use[29] and might be considered
213 to cover new areas of application. Strengthening the GABA response and inhibiting SGLT2 in
214 $CD4^+$ T cells might be valuable tools[30-32], when regulating inflammation is desirable.
215 In conclusion, physiological factors such as glucose, GABA and insulin guide the
216 adaptation of $CD4^+$ T cells and modify their effector functions. The reduction of metabolic
217 activity and release of inflammatory molecules in response to GABA or SGLT2 inhibitors,
218 revealed a switch that can be turned on or off. The study unveils the mechanisms of GABA
219 modulation of $CD4^+$ T cells and identifies a critical role for SGLTs in immune function. The
220 results have implications for treatment of a number of diseases including diabetes but also
221 maladies such as Covid-19 and cytokine storm, inflammatory diseases and cancer.
222
223 **Acknowledgements:** We thank the following for support; The Swedish Children's Diabetes
224 Foundation, The Swedish Diabetes Foundation, The Swedish Research Council, EXODIAB,
225 The Ernfors Foundation and The Thurings Foundation. We thank Dr Zhitao Gong for
226 participation in some of the experiments and Universitetslektor Femke Heindryckx for the gift
227 of the HepG2 cell line.
228 **Author Contributions:** BB, ZJ, HH conceived project; HH, ZJ, AKB, SVK, BB, MKM
229 designed experiments; HH, ZJ, AKB, SVK, OTR, SK, AIC and FA did experiments; ZJ, HH,
230 AKB, SVK made figures; all authors analyzed results, BB wrote manuscript that was edited by
231 ZJ, HH, AKB and then commented on by all authors.
232 **Competing interests**: BB has patent applications WO2019/164446A1 and WO2019162403A1
233

234 **References**

235 1 Geltink, R. I. K., Kyle, R. L. & Pearce, E. L. Unraveling the Complex Interplay Between T
236 Cell Metabolism and Function. *Annu Rev Immunol* **36**, 461-488 (2018).
237 https://doi.org:10.1146/annurev-immunol-042617-053019
238 2 van Niekerk, G., Christowitz, C., Conradie, D. & Engelbrecht, A. M. Insulin as an
239 immunomodulatory hormone. *Cytokine Growth Factor Rev* **52**, 34-44 (2020).
240 https://doi.org:10.1016/j.cytogfr.2019.11.006
241 3 Song, W., Li, D., Tao, L., Luo, Q. & Chen, L. Solute carrier transporters: the metabolic
242 gatekeepers of immune cells. *Acta Pharm Sin B* **10**, 61-78 (2020).
243 https://doi.org:10.1016/j.apsb.2019.12.006
244 4 Barragan, A., Weidner, J. M., Jin, Z., Korpi, E. R. & Birnir, B. GABAergic signalling in the
245 immune system. *Acta Physiol (Oxf)* **213**, 819-827 (2015).
246 https://doi.org:10.1111/apha.12467
247 5 Tian, J. & Kaufman, D. L. The GABA and GABA-Receptor System in Inflammation, Anti-
248 Tumor Immune Responses, and COVID-19. *Biomedicines* **11** (2023).
249 https://doi.org:10.3390/biomedicines11020254
250 6 Niswender, K. D. Basal insulin: physiology, pharmacology, and clinical implications.
251 *Postgrad Med* **123**, 17-26 (2011). https://doi.org:10.3810/pgm.2011.07.2300
252 7 Macintyre, A. N. *et al.* The glucose transporter Glut1 is selectively essential for CD4 T
253 cell activation and effector function. *Cell Metab* **20**, 61-72 (2014).
254 https://doi.org:10.1016/j.cmet.2014.05.004
255 8 Lunt, S. Y. & Vander Heiden, M. G. Aerobic glycolysis: meeting the metabolic
256 requirements of cell proliferation. *Annu Rev Cell Dev Biol* **27**, 441-464 (2011).
257 https://doi.org:10.1146/annurev-cellbio-092910-154237
258 9 Zhang, B. *et al.* B cell-derived GABA elicits IL-10(+) macrophages to limit anti-tumour
259 immunity. *Nature* **599**, 471-476 (2021). https://doi.org:10.1038/s41586-021-04082-1
260 10 Codo, A. C. *et al.* Elevated Glucose Levels Favor SARS-CoV-2 Infection and Monocyte
261 Response through a HIF-1alpha/Glycolysis-Dependent Axis. *Cell Metab* **32**, 498-499
262 (2020). https://doi.org:10.1016/j.cmet.2020.07.015
263 11 Wan, Q. *et al.* Recruitment of functional GABA(A) receptors to postsynaptic domains
264 by insulin. *Nature* **388**, 686-690 (1997). https://doi.org:10.1038/41792
265 12 Xu, E. *et al.* Intra-islet insulin suppresses glucagon release via GABA-GABAA receptor
266 system. *Cell Metab* **3**, 47-58 (2006). https://doi.org:10.1016/j.cmet.2005.11.015
267 13 Jin, Z. *et al.* Insulin reduces neuronal excitability by turning on GABA(A) channels that
268 generate tonic current. *Plos One* **6**, e16188 (2011).
269 https://doi.org:10.1371/journal.pone.0016188
270 14 Tsai, S. *et al.* Insulin Receptor-Mediated Stimulation Boosts T Cell Immunity during
271 Inflammation and Infection. *Cell Metab* **28**, 922-934 e924 (2018).
272 https://doi.org:10.1016/j.cmet.2018.08.003
273 15 Bhandage, A. K. *et al.* GABA Regulates Release of Inflammatory Cytokines From
274 Peripheral Blood Mononuclear Cells and CD4(+) T Cells and Is Immunosuppressive in
275 Type 1 Diabetes. *EBioMedicine* **30**, 283-294 (2018).
276 https://doi.org:10.1016/j.ebiom.2018.03.019
277 16 Cahalan, M. D. & Chandy, K. G. The functional network of ion channels in T
278 lymphocytes. *Immunol Rev* **231**, 59-87 (2009). https://doi.org:10.1111/j.1600-
279 065X.2009.00816.x

280 17 Vaeth, M., Kahlfuss, S. & Feske, S. CRAC Channels and Calcium Signaling in T Cell-
281 Mediated Immunity. *Trends Immunol* **41**, 878-901 (2020).
282 https://doi.org:10.1016/j.it.2020.06.012
283 18 Vaeth, M. *et al.* Store-Operated Ca(2+) Entry Controls Clonal Expansion of T Cells
284 through Metabolic Reprogramming. *Immunity* **47**, 664-679 e666 (2017).
285 https://doi.org:10.1016/j.immuni.2017.09.003
286 19 Pearce, E. L., Poffenberger, M. C., Chang, C. H. & Jones, R. G. Fueling immunity: insights
287 into metabolism and lymphocyte function. *Science* **342**, 1242454 (2013).
288 https://doi.org:10.1126/science.1242454
289 20 Jones, W. & Bianchi, K. Aerobic glycolysis: beyond proliferation. *Front Immunol* **6**, 227
290 (2015). https://doi.org:10.3389/fimmu.2015.00227
291 21 Traba, J., Miozzo, P., Akkaya, B., Pierce, S. K. & Akkaya, M. An Optimized Protocol to
292 Analyze Glycolysis and Mitochondrial Respiration in Lymphocytes. *J Vis Exp* (2016).
293 https://doi.org:10.3791/54918
294 22 Hummel, C. S. *et al.* Glucose transport by human renal Na+/D-glucose cotransporters
295 SGLT1 and SGLT2. *Am J Physiol Cell Physiol* **300**, C14-21 (2011).
296 https://doi.org:10.1152/ajpcell.00388.2010
297 23 Michalek, R. D. *et al.* Cutting edge: distinct glycolytic and lipid oxidative metabolic
298 programs are essential for effector and regulatory CD4+ T cell subsets. *J Immunol* **186**,
299 3299-3303 (2011). https://doi.org:10.4049/jimmunol.1003613
300 24 Fujii, S. & Beutler, E. High glucose concentrations partially release hexokinase from
301 inhibition by glucose 6-phosphate. *Proc Natl Acad Sci U S A* **82**, 1552-1554 (1985).
302 https://doi.org:10.1073/pnas.82.5.1552
303 25 Chang, C. H. *et al.* Posttranscriptional control of T cell effector function by aerobic
304 glycolysis. *Cell* **153**, 1239-1251 (2013). https://doi.org:10.1016/j.cell.2013.05.016
305 26 Young, S. Z. & Bordey, A. GABA's control of stem and cancer cell proliferation in adult
306 neural and peripheral niches. *Physiology (Bethesda)* **24**, 171-185 (2009).
307 https://doi.org:10.1152/physiol.00002.2009
308 27 Bailey, M. E., Albrecht, B. E., Johnson, K. J. & Darlison, M. G. Genetic linkage and
309 radiation hybrid mapping of the three human GABA(C) receptor rho subunit genes:
310 GABRR1, GABRR2 and GABRR3. *Biochim Biophys Acta* **1447**, 307-312 (1999).
311 https://doi.org:10.1016/s0167-4781(99)00167-0
312 28 Naffaa, M. M., Hibbs, D. E., Chebib, M. & Hanrahan, J. R. Pharmacological Effect of
313 GABA Analogues on GABA-varrho2 Receptors and Their Subtype Selectivity. *Life (Basel)*
314 **12** (2022). https://doi.org:10.3390/life12010127
315 29 Packer, M. *et al.* Cardiovascular and Renal Outcomes with Empagliflozin in Heart
316 Failure. *N Engl J Med* **383**, 1413-1424 (2020).
317 https://doi.org:10.1056/NEJMoa2022190
318 30 Espes, D. *et al.* GABA induces a hormonal counter-regulatory response in subjects with
319 long-standing type 1 diabetes. *BMJ Open Diabetes Res Care* **9** (2021).
320 https://doi.org:10.1136/bmjdrc-2021-002442
321 31 Masoodi, M. *et al.* Disturbed lipid and amino acid metabolisms in COVID-19 patients. *J*
322 *Mol Med (Berl)* (2022). https://doi.org:10.1007/s00109-022-02177-4
323 32 Alshnbari, A. & Idris, I. Can sodium-glucose co-transporter-2 (SGLT-2) inhibitor reduce
324 the risk of adverse complications due to COVID-19? - Targeting hyperinflammation.
325 *Curr Med Res Opin* **38**, 357-364 (2022).
326 https://doi.org:10.1080/03007995.2022.2027141

Figure 1

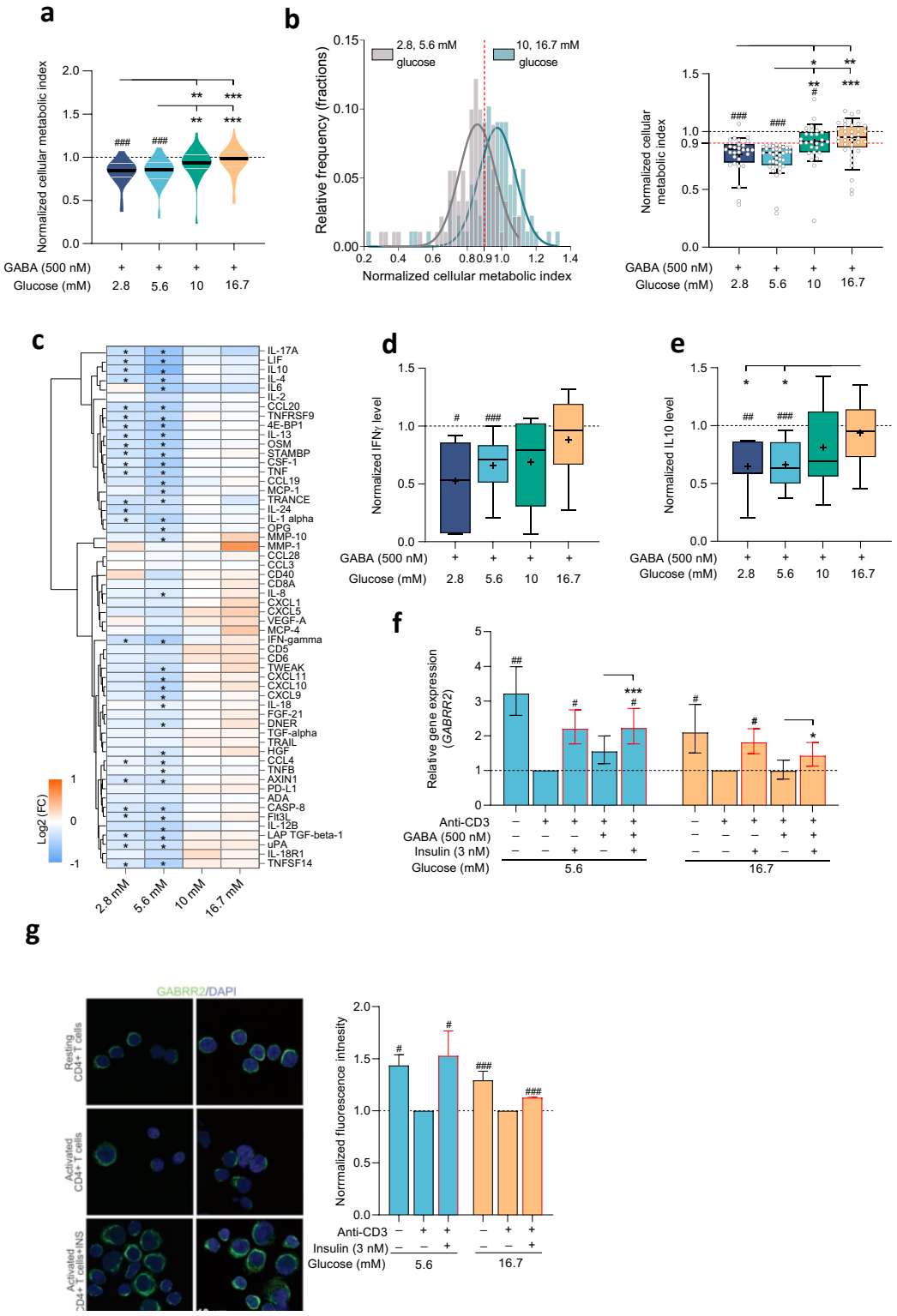

327
328
329

Figure 1. GABA effects on metabolic activity and cytokine release are glucose concentration-dependent in activated $CD4^+$ T cells.

a, Cellular metabolic activity, glucose (mM): 2.8 (N=36), 5.6 (N=54), 10 (N=35) and 16.7 (N=53). Violin plots where horizontal black and grey lines indicate the median and quartiles.

b, Left panel. Histograms of normalized cellular metabolic activity at low-normal (2.8 and 5.6) and high (10 and 16.7) glucose concentrations (mM). Solid lines: Gaussian fits, vertical broken line: 10% inhibition by GABA (500 nM). Right panel. Metabolic activity of cells from donors where ≥10% GABA inhibition was observed at 5.6 mM glucose; 2.8 (N=28), 5.6 (N=37), 10 (N=27) and 16.7 (N=36).

c, Heatmap and hierarchical clustering of biomolecules by PEA 72 h post-stimulation of cells (N=17). Data represent the mean log2 (fold change) for samples cultured in presence and compared to absence of GABA.

d, e, GABA effect on IFNγ **(d)** and IL-10 **(e)** release. ELISA, 72 h post-stimulation, glucose (mM): 2.8 (N=7;7), 5.6 (N=17;17), 10 (N=6;10) and 16.7 (N=16;16).

f, Relative expression of *GABRR2* mRNA in resting and activated cells in 5.6- or 16.7-mM glucose (N=6) analyzed by $2^{-\Delta\Delta Ct}$ method.

g, Immunofluorescence co-staining of GABRR2 (green) and DAPI (blue), 5.6- or 16.7-mM glucose. Bar graph; normalized GABRR2 fluorescence intensity (n>50 cells/group, N=3).

Data were normalized to values of activated cells in the absence of drugs at each glucose concentration (**a, c, e, f, g**). Data represent geometric mean ± SEM in (**f**), mean ± SEM in (**g**). Box and whisker (**c, e, f**): 10-90 percentiles, means: +, medians: black lines in the boxes. Statistics: one sample t-test when compared to activated cell group (#, $p<0.05$; ##, $p<0.01$; ###, $p<0.001$), paired groups by repeated measures ANOVA or fitting a mixed-effects model, or ordinary one-way ANOVA followed by Tukey (**a, c, e, f**) or Fisher's LSD test (**g**) for multiple comparisons (*, $p<0.05$; **, $p<0.01$; ***, $p<0.001$). Statistical significance in **c** ($p \leq 0.05$ and adjusted p-value $q < 0.12$) are marked with *. **N**: donors.

Figure 2

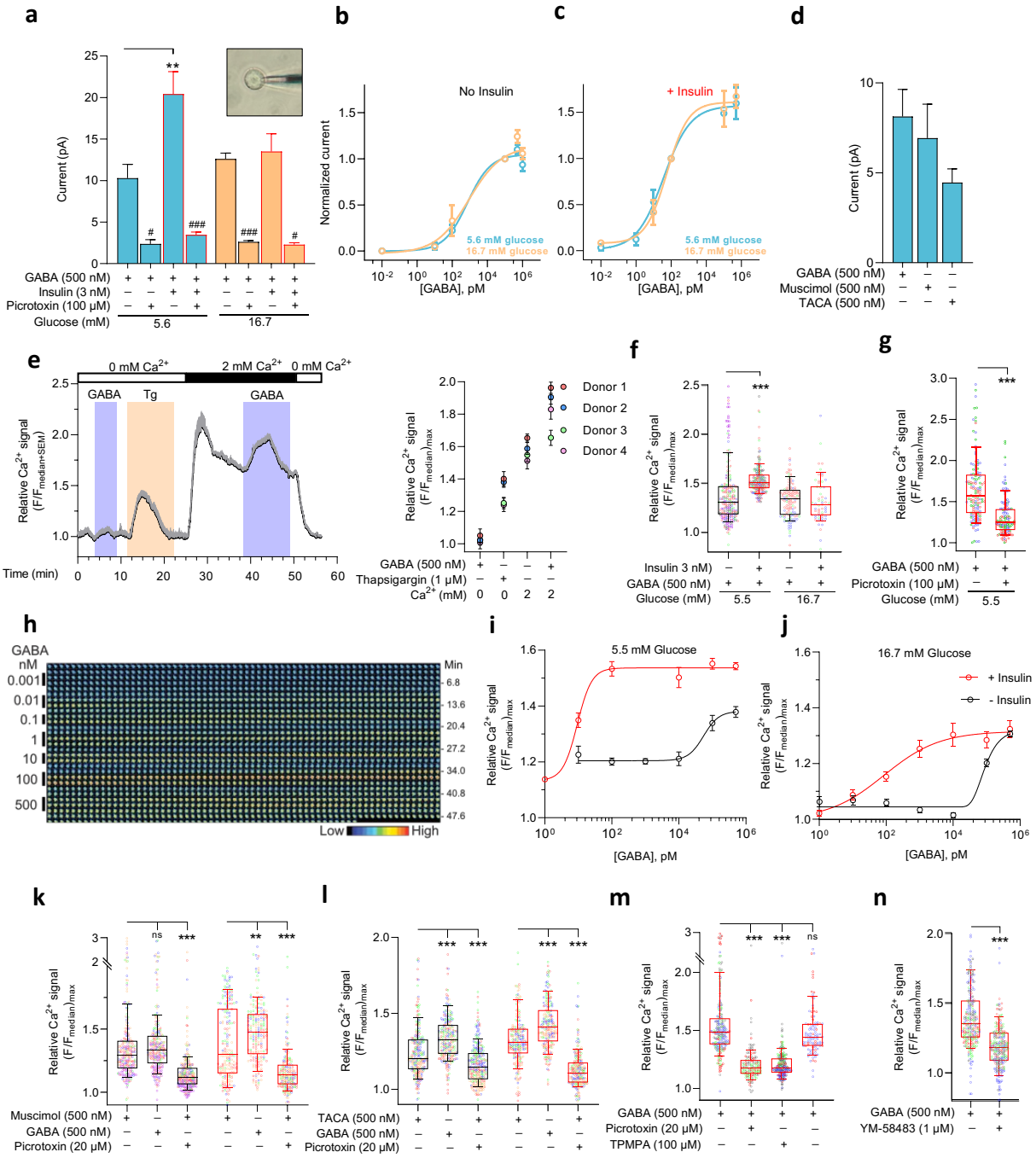

360
361

Figure 2. Insulin enhances GABA-activated $GABA_AR$ currents and Ca^{2+} entry in activated $CD4^+$ T cells.

a, GABA-activated whole-cell currents (n=3-8, N=11). Insert: a patch-pipette attached to an activated $CD4^+$ T cell.

b, c, GABA dose-response curves in cells without (b) or treated with (c) insulin. The currents were normalized to 100 nM (b) or 100 pM (c) GABA responses (n=3-11, N=27).

d, Whole-cell currents evoked by GABA (n=11, N=9), muscimol (n=4, N=3) or TACA (n=5, N=4), 5.6 mM glucose.

e, Left panel: Mean Ca^{2+} signal intensity trace (black dots) and SEM (gray whiskers) recorded 72 h after activation of cells (n=14). Colored bars: Perfusion time of drugs (GABA 500 nM and thapsigargin, Tg 1 μM) in 0 or 2 mM Ca^{2+}-containing perfusion medium. Right panel: Relative Ca^{2+} signal (mean ± SD) (n=14, 20, 41, 47, N= 4).

f, GABA-activated relative Ca^{2+} signal (n=58-232, N=3-5) without or treated with insulin.

g, GABA-activated relative Ca^{2+} signal in cells (n=131, N=3) in absence or presence of picrotoxin, with insulin.

h, Representative time-lapsed micrographs of a live Ca^{2+} imaged cell (16.7 mM glucose, with insulin). GABA concentrations were sequentially perfused and inter-spaced with medium applications. Color scale: Relative fluorescence intensity.

i, j, Dose-response relationship for GABA-induced Ca^{2+} signals (n=63-279, N=3-8), see also ~~Figure~~ Extended Data 2e.

k, l, m, n, Effects of $GABA_AR$ agonists and antagonists on the relative Ca^{2+} signal: muscimol, TACA, picrotoxin, TPMPA and SOCE antagonist YM48583, 5.5 mM glucose. Box plots; black without and red with insulin, 5.5 mM glucose, (n=191-265, N=3-5).

Curve fitting (**b, c, i, j**): nonlinear regression with sigmoidal polynomial (4PL) model. Data presented as mean ± SEM (**a, b, c, d, i, j**). Statistics: ordinary one-way ANOVA (**a, d**) or repeated measures ANOVA followed by Tukey multiple comparison test (**k, l, m**) or unpaired (**f**) or paired (**g, n**) student's t-test. ns, $p > 0.05$; **, $p < 0.01$; ***, $p < 0.001$. #, $p< 0.05$; ###, $p< 0.001$ – picrotoxin vs. respective group before picrotoxin application. **n**: cells, **N**: donors.

Figure 3

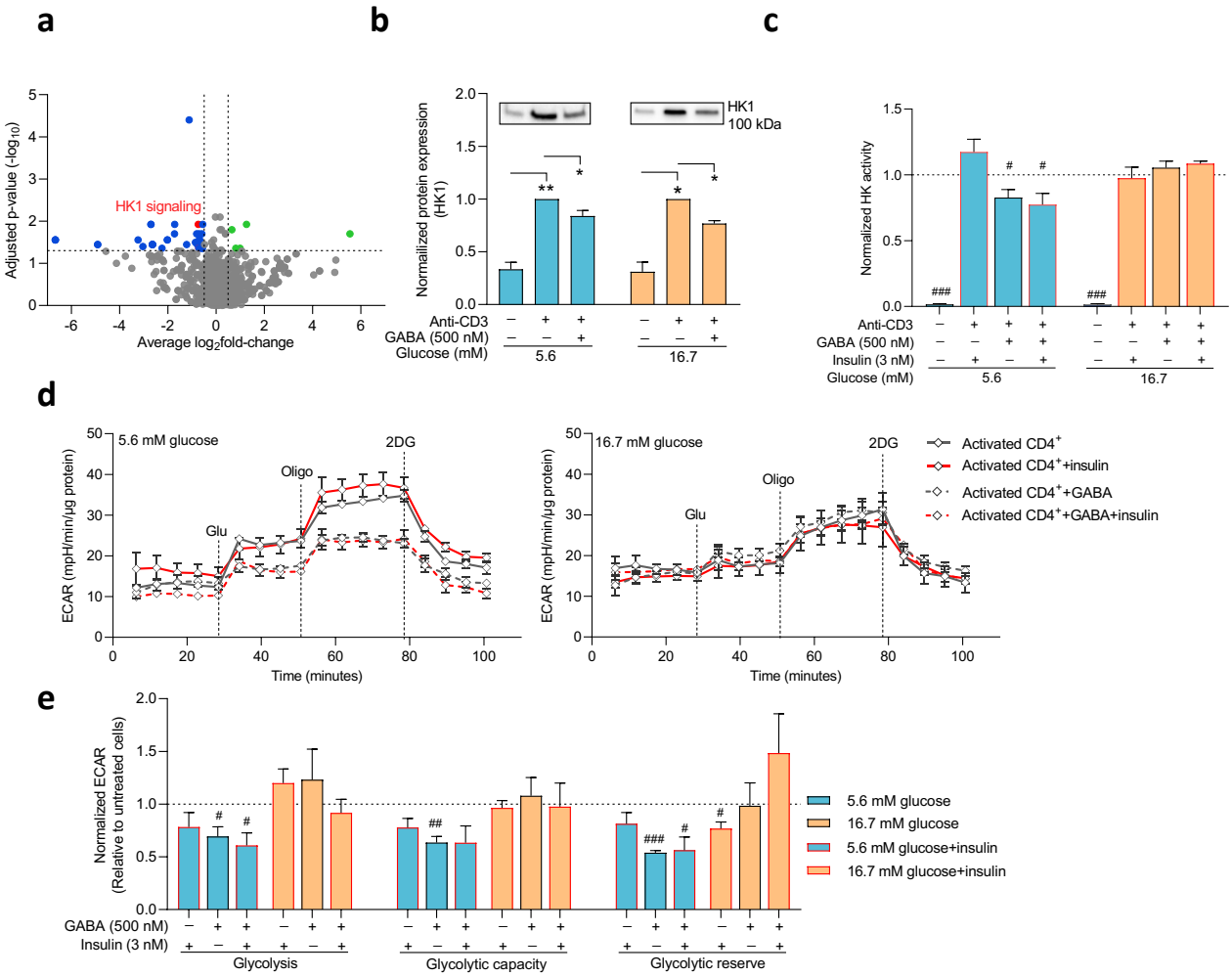

Figure 3. GABA inhibits hexokinase and glycolysis in activated CD4⁺ T cells.
a, The volcano plot summarizes pathways that are significantly up- (green) or down-regulated (blue and red (HK1)) by GABA treatment in cells 72 h post activation (N=5), 5.6 mM glucose. The x-axis represents the average $\log_2$ fold-change of all proteins measured by mass spectrometry within that pathway and every dot is one pathway. The y-axis represents the adjusted p-value (–log10 transformation). The horizontal line represents p = 0.05, and the vertical lines represent average log2 (fold change) <–0.5 or >+0.5.
b, Western blot images and relative expression of HK1 protein (N=7 at 5.6 mM and 3 at 16.7 mM).
c, *In vitro* HK activity analyzed in resting and activated cells, 5.6 mM (N=12) or 16.7 mM (N=6) glucose. HK activity (µmol NADH/min/ml) was normalized to the activity of activated cells in the absence of drugs.
d, Representative ECAR over time in cells 72 h post-activation treated with or without GABA (500 nM) or insulin at 5.6 mM (left panel) or 16.7 mM (right panel). Dashed lines indicate injections of glucose (Glu.), oligomycin (Oligo) or 2-deoxyglucose (2-DG) into media.
e. ECAR results (mpH/min/protein) were normalized to controls in absence of drugs for average glycolysis, glycolytic capacity and glycolytic reserve in cells 72 h post-activation treated with or without GABA or insulin, 5.6 mM (N=5) or 16.7 mM (N=5) glucose.
Data are normalized to values of activated cells in the absence of drugs at each glucose concentration (**b, c, e**). Data represent mean ± SEM (**b, c, d, e**). Statistics by one sample t-test when compared to activated cell group (#, p<0.05; ##, p<0.01; ###, p<0.001), repeated measures ANOVA or fitting a mixed-effects model followed by Tukey multiple comparison test. **N**=donor.

Figure 4

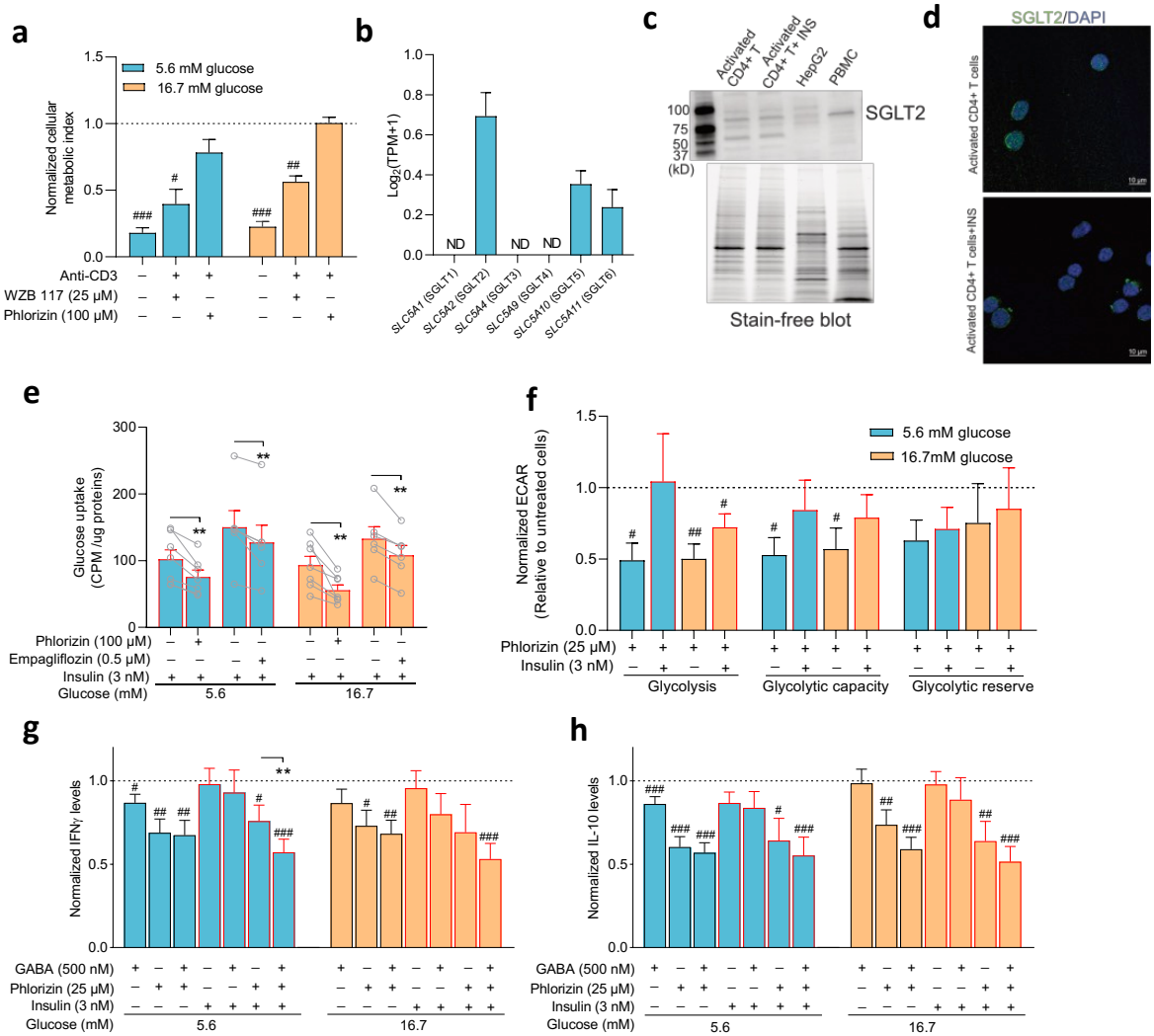

Figure 4. SGLT2 is expressed, functional and modulates glycolysis and release of IFNγ and IL-10 in activated CD4⁺ T cell.

a, The cellular metabolic activity of resting and activated cells in presence of GLUT1 inhibitor, WZB 117 or SGLTs inhibitor, phlorizin was normalized to that of activated cells without drug treatment at 5.6 mM or 16.7 mM glucose (N=4).

b, Relative gene expression levels of Na^+-dependent glucose transporters in activated cells at 5.6 mM glucose (N=6) determined by RNAseq analysis. TPM, transcripts per million. ND, not detected.

c, Representative Western blot image of SGLT2 protein in activated $CD4^+$ T cells and HEPG2 cell line. The stain-free blot image represents total proteins loaded for each sample, insulin (3 nM), 16.7 mM glucose.

d, Representative immunofluorescence co-staining of SGLT2 (green) and DAPI (blue) in $CD4^+$ T cells, 5.6 mM or 16.7 mM glucose.

e, Glucose uptake in absence or presence of phlorizin (N=9) and SGLT2 selective inhibitor, empagliflozin (N=6) in cells 72 h post-activation, insulin, 5.6 mM or 16.7 mM glucose.

f, ECAR results (mpH/min/protein) normalized to untreated cells for average glycolysis, glycolytic capacity and glycolytic reserve in cells, 72 h post-activation, incubated with phlorizin, with or without insulin in 5.6 mM (N=5) or 16.7 mM (N=5) glucose.

g, h, IFNγ **(g)** and IL-10 **(h)** release from activated cells 72 h post-activation in with or without GABA, phlorizin or insulin, at 5.6 mM or 16.7 mM glucose (N=17).

Data represent mean ± SEM. Data are normalized to values of activated cells in the absence of drugs at each glucose concentration (**a, e, f, g, h**). Statistics by one sample t-test when compared to activated cell group (#, $p<0.05$; ##, $p<0.01$; ###, $p<0.001$), repeated measures ANOVA or fitting a mixed-effects model followed by Tukey multiple comparisons test, *, $p<0.05$. **N**=donor.

Extended Data

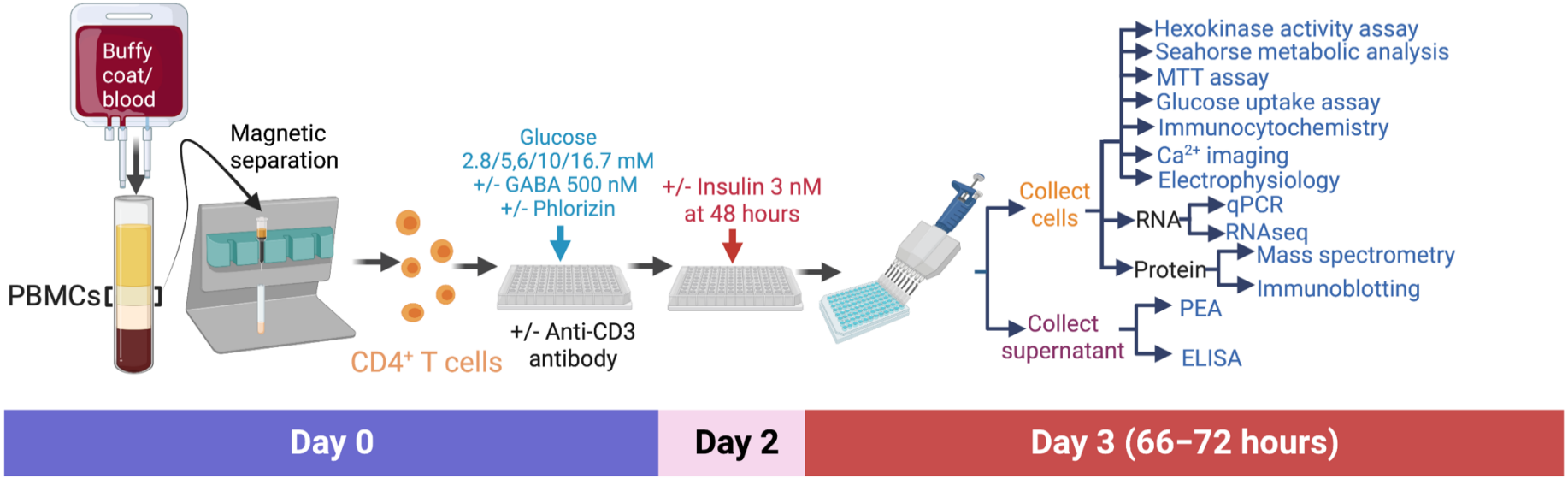

Extended Data Fig. 1: Schematic diagram of the experimental design.
Created with BioRender.com.

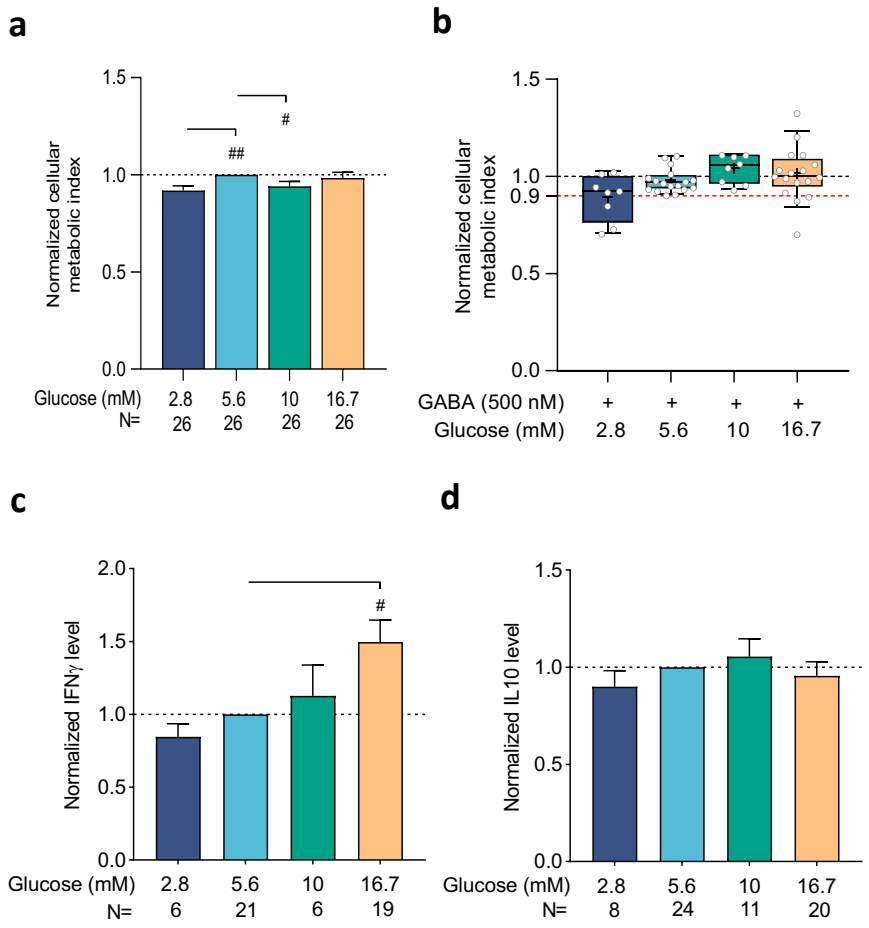

Extended Data Fig. 2: The effect of glucose on cellular metabolic activity and release of IFNγ and IL-10 from CD4⁺ T cells.

a, Cellular metabolic activity from donors where <10% GABA inhibition at 5.6 mM glucose was observed. **b,** Cellular metabolic activity of CD4⁺ T cells 72 h after activation in the presence of different glucose concentrations. **c, d,** IFNγ (**c**) and IL-10 (**d**) released from CD4⁺ T cells 72 h after activation in presence of different glucose concentrations. Data are normalized to values at 5.6 mM glucose and presented as mean ± SEM. Statistics by one sample t-test when compared to 5.6 mM glucose group (#, $p<0.05$; ##, $p<0.01$), repeated measures ANOVA or fitting a mixed-effects model followed by Tukey test for multiple comparisons. N = number of donors.

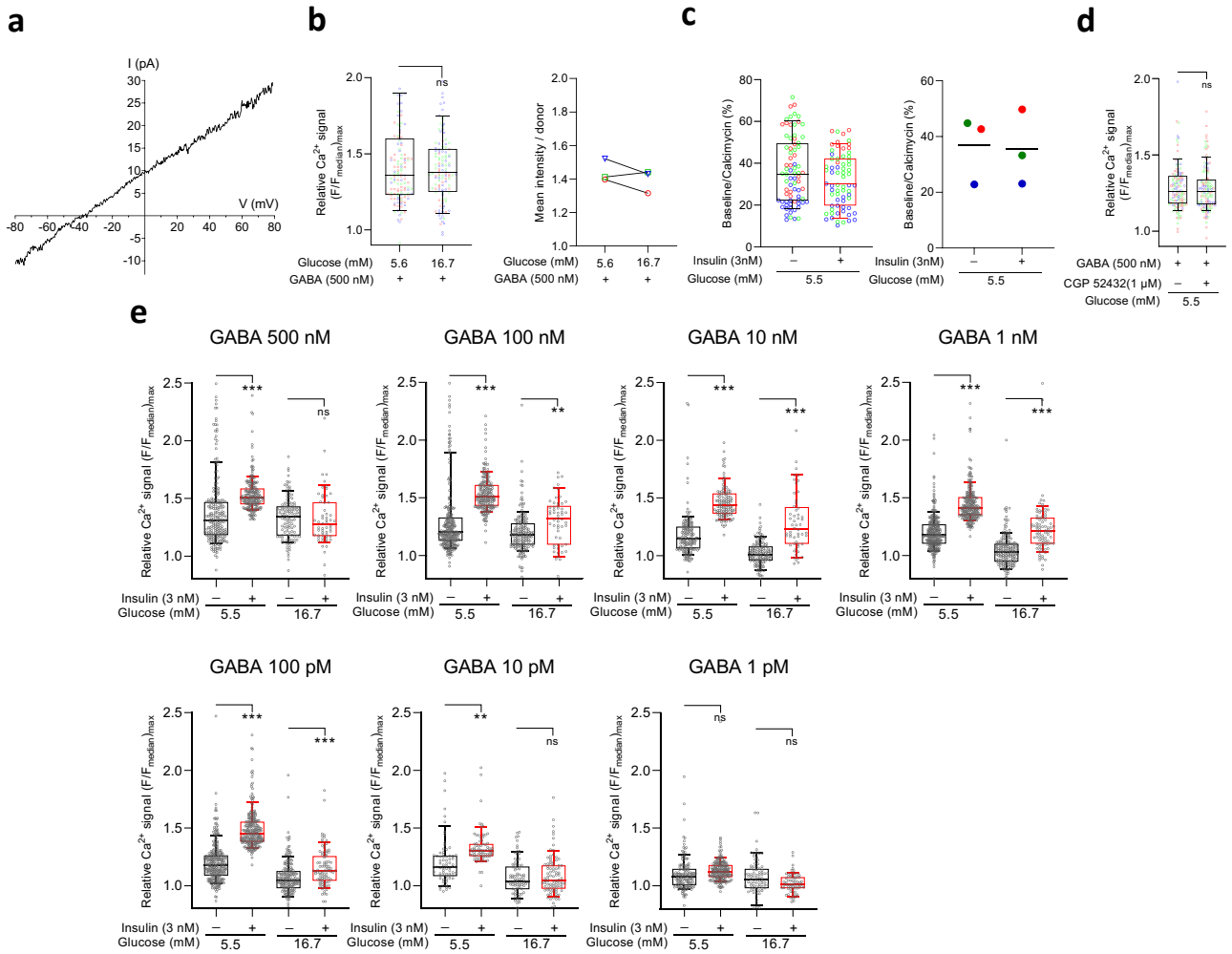

Extended Data Fig. 3: GABA-activated current and Ca^{2+} signaling in $CD4^+$ T cells.
a, A representative current-voltage relationship recorded in an activated $CD4^+$ T cell in response to 500 nM GABA application by perforated patch-clamp, 5.6 mM glucose. **b,** GABA (500 nM)-activated relative Ca^{2+} signals (left panel) and mean intensity (right panel) recorded from activated $CD4^+$ T cells (n=128 cells/ N=3 donors) in sequentially applied 5.6 mM and 16.7 mM glucose-containing media. Cells were activated in 5.5 mM glucose-containing media for 72 h. **c,** The ratio of Ca^{2+} signals in the absence and presence of calcium-ionophore calcimycin (1 ⍰M) in $CD4^+$ T cells (n=85 cells/ N=4 donors) 72 h after activation with or without insulin treatment. **d,** GABA-activated relative Ca^{2+} signal recorded in $CD4^+$ T cells (n=131 cells/ N=3 donors) in the absence or presence of $GABA_B$ receptor antagonist CGP 52432 (1 μM) at 5.5 mM glucose. **e,** Relative Ca^{2+} signals induced by different concentrations of GABA in activated $CD4^+$ T cells treated without or with insulin in 5.5 mM or 16.7 mM glucose (n=63-279 cells/ N=3-8 donors). Statistics by two-tailed student's t-test. ns, $p > 0.05$, **, $p<0.01$; ***, $p<0.001$.

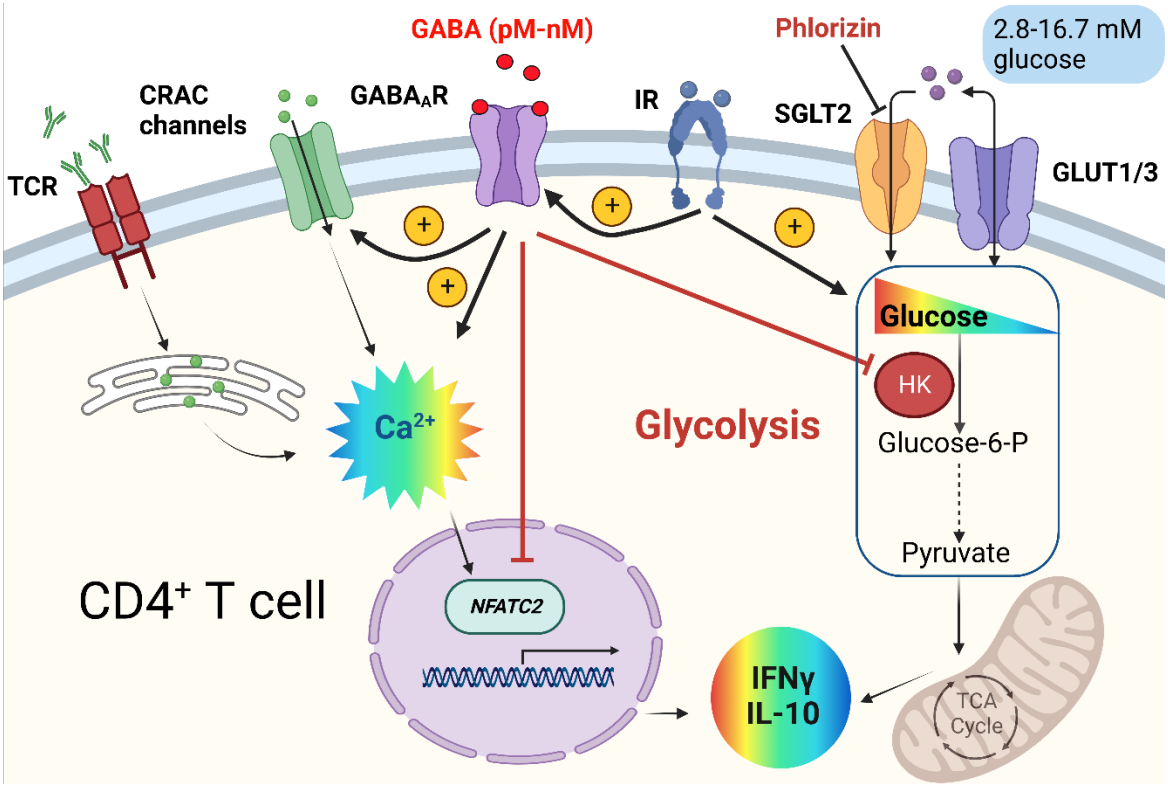

Extended Data Fig. 4: GABA, glucose and insulin regulate CD4+ T cell effector functions. In human CD4+ T cells, the activation of T cell receptor (TCR)/CD3 complex by anti-CD3 antibodies binding, initiates store-operated Ca2+ entry (SOCE) through Ca2+ release-activated Ca2+ (CRAC) channels. It regulates intracellular Ca2+ signals, drives changes in transcription factors, upregulates glycolysis and increases T cell effector functions. Physiological concentration of GABA (pM-nM) activates GABAA receptors (GABAAR) to modulate T cells metabolic activity and levels of cytokines (e.g., IFNγ and IL-10) by 1) enhancing function of CRAC channels and Ca2+ entry; 2) reducing expression of Nuclear Factor of Activated T cell 2 (NFATC2 or NFAT1); 3) decreasing expression and activity of hexokinase (HK), the 1st rate-limiting enzyme in aerobic glycolysis. In addition, insulin-insulin receptor (IR) signaling promotes glycolysis but paradoxically reduce glycolysis by enhancing GABAAR function. The fluctuation of blood glucose concentration affects glycolysis and cytokine production. Glucose uptake is mediated by not only the facilitated glucose transporters GLUT1/3 but also the sodium-dependent glucose transporter 2 (SGLT2). Phlorizin, a SGLT inhibitor, reduces glucose uptake, attenuates glycolysis and reduces IFNγ and IL-10 levels.
Created with BioRender.com.

Extended Data Table 1 | Donors' demographic information

Parameter	Normal Donors (N=160)
Age (years)	26.2 ± 0.25
Sex (N, %)	89 males (55.6%)
	71 females (44.4%)

Data are presented as means ± SEM.

Extended Table 2 I Relative gene quantification (normalized to activated cells) by qPCR (N=7-11 donors).

Gene name	5.6 mM glucose					16.7 mM glucose				
	Resting	Activated	Activated+Insulin	GABA	GABA+Insulin	Resting	Activated	Activated+Insulin	GABA	GABA+Insulin
NFATC1	0.088	1***	1.129***	1.086**	1.140***	1.902	1**	1.017	1.072*	0.923**
NFATC2	0.996	1	0.980	0.884$^{\#\#}$	0.942	1.333	1	0.961$^{\&}$	1.121	0.876$^{*, \&}$
NFATC3	0.512	1**	0.929**	0.836*	0.773**	0.484	1*	0.895$^{*, \&}$	1.057**	0.922*
JAK1	1.808	1***	1.156	1.096***	1.144$^{***, \#}$	2.123	1	1.049	1.329	1.027
JAK2	0.405	1***	1.060***	1.085***	1.133***	0.291	1	0.802	1.041	0.932
TYK2	1.639$^{\#}$	1	1.278	1.016	0.997*	1.254	1	0.716	0.826	0.596
HIF1A	0.310	1***	1.005***	0.961***	0.960***	0,287	1***	0.919***	0.968***	0.794***
STAT1	0.088	1***	1.129$^{***, \#}$	1.086***	1.140***	0.067	1***	0.939***	0.925***	0.981***
MYC	0.626	1**	0.925**	0.918*	0.946**	0.368	1**	0.662$^{\#}$	0.805*	0.787*

*p<0.05, **p<0.01, ***p<0.001, as compared to resting cells; #p<0.05, ##p<0.01, as compared to activated cells: &p<0.05, as compared to GABA-treated cells. The statistical analysis was performed on ΔCq values with repeated measures one-way ANOVA with Fisher's LSD test for multiple comparison.

Extended Data Table 3 | Reactome analysis of MS data (N=5 at 5.6 mM glucose). Proteins are named after UniProtKB.

Top up-regulated proteins

Identifier	logFC	AveExpr	t	P.Value
K2C79_HUMAN	0.67266061	13.2926208	2.34394122	0.04308325
CHM4A_HUMAN	0.55827697	13.7149206	2.20925349	0.05380739
HLAH_HUMAN	1.03346983	14.8113954	2.03947592	0.07106636
RAB2A_HUMAN	1.37200668	14.1750267	2.03797883	0.07123998
SC11A_HUMAN	5.70132617	10.587487	1.91122932	0.08749562
K22O_HUMAN	0.48972535	12.2546633	1.88242372	0.09164997
DYL1_HUMAN	5.54957599	10.7818438	1.81112175	0.10274055
PLXA4_HUMAN	0.69449352	13.706242	1.7195177	0.11881622
RL36_HUMAN	6.02123532	12.32297	1.68555819	0.12534011
IF4G2_HUMAN	0.82748497	13.4787932	1.68221061	0.12600056

Top down-regulated proteins

Identifier	logFC	AveExpr	t	P.Value
TBB1_HUMAN	-7.55965074	8.58464831	-2.74841088	0.02204275
STA5B_HUMAN	-7.60692039	6.04448902	-2.44305026	0.03656351
EXOS3_HUMAN	-6.6014009	5.67159622	-2.16624065	0.05775108
BGAL_HUMAN	-6.67048214	5.77846898	-2.13711593	0.06057899
AL1B1_HUMAN	-6.67577438	5.87276979	-2.08793829	0.06566002
HXK1_HUMAN	-0.73989819	14.3697968	-2.06803575	0.06783079
HLAG_HUMAN	-6.34860408	5.64345434	-2.03980339	0.07102844
COPG1_HUMAN	-5.15586276	10.0461233	-1.80136877	0.10435116
BCL2_HUMAN	-4.91388319	9.86964223	-1.73134501	0.11661798
PIP_HUMAN	-4.68190741	9.67505331	-1.66669489	0.12910318

Methods

Study individuals and collection of samples

Human blood buffy coat and blood samples were obtained from Uppsala University Hospital (Uppsala Akademiska sjukhuset), protocol approved by the Regional Research Ethical Committee in Uppsala. All donors were voluntary recruited and informed consent were signed. In total, samples from 160 normal donors, 89 men and 71 women with mean age 26.2 ± 0.25 years were included in the study.

Chemicals and reagents

Drugs, buffers and salts unless otherwise specified were purchased from Sigma-Aldrich/Merck (Steinheim, Germany). TACA, muscimol, TPMPA, YM-58483, WZB 117 were purchased from Tocris (UK, 7A/109031). Phlorizin and empagliflozin were obtained from AdooQ Bioscience. Urea and NH_4HCO_3 were from Acros Organics, Geel, Belgium and trypsin and dimethyl sulfoxide (DMSO) from Thermo Scientific (Waltham, MA). Tris(hydroxymethyl) aminomethane hydrochloride (Tris), LC-MS grade water, acetonitrile and formic acid were obtained from Fisher Scientific (Geel, Belgium).

$CD4^+$ T cells isolation and activation

Peripheral blood mononuclear cells (PBMCs) were isolated by density-gradient centrifugation using Ficoll-Paque™ PLUS (Sigma Aldrich, Sweden). $CD4^+$ T cells were then purified from the isolated PBMCs by negative selection using human$CD4^+$ T cell isolation kits (Miltenyi Biotec, Germany) according to the manufacturer's instructions. The freshly isolated $CD4^+$ T cells (1x 10^6/ml) were suspended in RPMI 1640 glucose-free medium (Gibco, Fisher Scientific, Sweden) supplemented with 2 mM glutamine, 10% heat-inactivated dialyzed fetal bovine serum, 100 U/ml penicillin, 10 mg/ml streptomycin, and 5 μM β-mercaptoethanol (Gibco, Fisher Scientific, Sweden). The activation of the cells was performed in either 96-well (10^5 cell/well) or 24-well (10^6 cell/well) plates based on the purpose of the experiment. $CD4^+$ T cells were activated with 3 μg/ml plate-bound anti-CD3 (BD Biosciences, USA, 555329) in the presence of different concentrations of glucose (2.8 mM, 5.6 mM, 10 mM and 16.7 mM) for 66–72 h and indicated drugs were added based on the experimental design.

MTT Assay

The metabolic activity of $CD4^+$ T cells was assessed in 96-well plates with colorimetric MTT (3-(4,5-Dimethylthiazol-2-yl)-2,5-Diphenyltetrazolium Bromide) assay. After 66–72 h of activation, a PBS-soluble tetrazolium dye MTT (final concentration 1mM) was added and incubated for additional 4 h at 37 °C. Thereafter, the cells were centrifuged at 2000 rpm for 10 min to concentrate the insoluble purple formazan pellets. The supernatants were collected and stored at −80 °C for later biomolecules analysis. The formazan crystal pellets were dissolved in DMSO and the plate was read 10 min later using Multiskan FC Microplate Photometer (Thermo Fisher, USA) at 550 nm.

Multiplex Proximity Extension Assay (PEA)

The supernatants collected at the end of the MTT assay were sent on-ice to the SciLifeLab Affinity Proteomics Unit in Uppsala, Sweden, for analysis. Inflammatory proteins were measured using high-throughput multiplex PEA with an Olink Target 96 Inflammatory panel (OlinkProteomics, Uppsala, Sweden). PEA measures simultaneously 92 proteins/biomolecules in different sample matrices where it

combines a dual-detection immunoassay and quantitative PCR. Normalized protein expression (NPX) values, an arbitrary unit on the log2 scale, were used to present the data. A protein expression (NPX value) is considered acceptable if the value is above the limit of detection (LOD) for each particular protein. Proteins that were detected in more than 75% of the samples were analyzed in this study: 59 out of 92 proteins had detectable levels. Data for resting, activated and GABA-treated activated $CD4^+$ cells supernatants were analyzed separately. The biomolecules in the supernatants were assessed for each donor at each glucose concentration. The data was computed, processed and analyzed with support from NBIS (National Bioinformatics Infrastructure Sweden). The log2FC (FC =fold change) is the average increase in NPX in GABA as compared to activated alone, this value is both estimated based on the linear mixed effects model and computed as the mean over the GABA-activated difference and plotted in heatmaps. Paired t-test was used followed by multiple testing correction using false discovery rate (FDR) method (Two-stage step-up method of Benjamini, Krieger and Yekutieli) with a threshold 12%.

Determination of IFNγ and IL-10 concentrations in supernatants

The concentrations of IFNγ and IL-10 were measured with enzyme-linked immunosorbent assay (ELISA). The supernatants were diluted when necessary to be in the optimal linear optical range and analyzed using commercial kits for IFNγ (Human IFN-gamma DuoSet ELISA, R&D Systems, USA and Bio legend, UK), and IL-10 (Biolegend, UK) according to manufacturers´ instructions. Optical densities were measured using FC Microplate Photometer (Thermo Fisher, USA) at 450 nm, and 540 nm was used as a correction wavelength. The levels of IFNγ or IL-10 were normalized to controls (activated $CD4^+$ T cells in the absence of drugs).

Total RNA and protein extraction and, bulk RNA sequencing

Total RNA and protein were extracted from activated $CD4^+$ T cells, in the absence or presence of 500 nM GABA, using RNA/Protein Purification Plus Kit (Norgen Biotek, Ontario, Canada). During the extraction process, total RNA was treated with RNase-Free DNase I Kit (Norgen Biotek, Ontario, Canada) to eliminate contamination of genomic DNA. The extracted proteins were quantified using DC protein assay kit (Bio-Rad, USA), and immediately frozen at −80°C. Total RNA samples were submitted to the GENEWIZ NGS facility (Germany) and quality control analysis showed that all RNA samples had an RNA integrity number (RIN) >9 (9.48 ± 0.1, mean ± SEM). Strand-specific RNAseq cDNA libraries with polyA selection were generated and sequenced using Illumina HiSeq sequencing platform (12 samples, 20.8-31.1 million reads, 150 bp paired end per sample). Sequence reads were filtered and trimmed using Trimmomatic V.0.36 to remove low quality reads. The trimmed reads were further mapped and aligned to the Homo Sapiens GRCh38 reference genome (ENSEMBL) using the STAR aligner v.2.5.2b. Unique gene hit counts were calculated using feature Counts from the Subread package v.1.5.2.

Real-Time Quantitative Reverse Transcription (qPCR)

The cDNA was synthesized using SuperScript reverse transcriptase IV (Invitrogen Thermo Scientific, USA) in a 20 µl reaction following the standard protocol from manufacturer. The qPCR reaction was then performed using qPCRBIO SYBR or Probe Mix low-ROX (PCR Biosystems, UK; PB20.11-05), and gene-specific primers (Table S1) or Taqman probes (*GABRR2* Hs00266703_m1; *IPO8* Hs00914057_m1, ThermoFisher Scientific, USA). Changes in the abundance of each transcript were normalized to the expression of reference genes (*IPO8*). Relative expression levels

were calculated by normalizing to non-treated activated $CD4^+$ T cells obtained from the same donor at the same glucose concentration using $2^{-\Delta\Delta Ct}$ method. All samples were run in duplicate. The real-time qPCR amplification was performed in 10 µl reaction mix in a 384-well plate usings a QuantStudio™ 5 instrument (ThermoFisher Scientific). All runs started with an initial denaturation step of 2 min at 95 °C, followed by 45 cycles of 95 °C for 5 s and 60 °C for 30 s.

Mass spectrometry (MS)-based bottom-up proteomics

The lysates were purified and tryptic digested for MS-based bottom-up proteomic analysis using Filter Aided Sample Preparation (FASP)[1, 2]. Briefly, 20 µg of total protein were transferred onto centrifugal filter units (Microcon-30 kDa; Merck, Darmstadt, Germany) and washed with a buffer containing 8 M urea and 100 mM Tris (pH 8.5). The washing step was repeated after reduction with 8 mM dithiothreitol (DTT), alkylation with 50 mM iodoacetamide (IAA) and removal excess of IAA with 8 mM DTT. Before tryptic digestion (enzyme-to-protein ratio 1:50 (w/w)) the filter was washed three times with NH_4HCO_3. After incubation in a wet chamber at 37 °C for 16 h the resulting peptides were washed twice from the filter by adding 50 mM NH_4HCO_3. Trifluoroacetic acid was then added to a final concentration of 1% (v/v) and the samples were dried at 45 °C. Finally, the samples were reconstituted in 3% acetonitrile and 0.1% formic acid in water to a final concentration of 150 ng protein/µl. The tryptic peptides were analyzed on a nanoAcquity UPLC system equipped with a C18, 5 µm, 180 µm x 20 mm trap column and an HSS-T3 C18 1.8 µm, 75 µm x 250 mm analytical column (Waters Corporation, Manchester, UK) coupled to a Synapt G2 Si HDMS mass spectrometer with an electrospray ionization source (Waters Corporation, Manchester, UK). The $UDSM^E$ approach with positive ionization was used[1, 2]. Mobile phase A contained 3 % DMSO and 0.1 % formic acid in water and mobile phase B 3 % DMSO and 0.1 % formic acid in acetonitrile. After loading 300 ng of protein on the column in trapping mode, peptide separation was performed with a gradient run from 3 - 40% (v/v) mobile phase B over 120 min. The flow rate was set to 0.3 µl/min and the column oven was set to 40 °C. Method performance was controlled with a commercially available HeLa digest (Thermo Scientific, Waltham, MA). UPLC-MS data processing and label-free quantification: ProteinLynx Global Server (version 3.0.3, Waters Corporation, Milford, MA) was used for raw data processing. With FDR of 10%, a database search against a randomized UniProt human database (Uni-ProtKB version 14/01/2020) was performed. Carbamidomethyl cysteine was set as fixed modification, acetyl lysine, C-terminal amidation, asparagine deamidation, glutamine deamidation and methionine oxidation as variable modifications and trypsin as digest reagent. Minimum peptide matches per protein were 2 and minimum fragment ion matches per peptide and protein were 1 and 3, respectively. For label-free quantification analysis, the identified proteins were further processed using ISOQuant 1.8 as described elsewhere[2]. Following the TOP3 quantification approach the average intensity of the three most intense peptides of each protein were used for relative protein quantification. ISOQuant settings are provided in Table S2.

Immunoblotting

$CD4^+$ T cells were lysed in RIPA buffer (Sigma-Aldrich, R0278) containing protease inhibitor cocktail (Roche, 11 836 153 001) and phosphatase inhibitors (Sodium orthovanadate, Sigma-Aldrich, S6508). Proteins were heated at 100 °C for 5 min in SDS loading buffer (275 mM Tris. HCL, 9% SDS, 50% glycerol, 0.03% bromophenol

blue) containing 9% beta-mercaptoethanol and separated by Mini-Protean TGX gel 4 - 15% (BioRad, stain-free gels #4568084, 4561035) and blotted onto Amersham Hybond-P PVDF membrane. Membranes were blocked with blocking buffer (EveryBlot BioRad, 12010020) for 20 min at room temperature (RT) and incubated overnight at 4 °C with the following primary antibodies: HK1 (GenTex, GTX105248, 1:3000), SGLT2 (ProteinTech, 24654-1-AP, 1:500) and GABRR2 (Invitrogen, PA5-41008, 1:1000). After immunoblotting, membranes were washed in TBST and incubated with Peroxidase-conjugated AffiniPure secondary antibodies (Jackson ImmunoResearch, 111-035-045, 1:5000). Protein detection was done using chemiluminescent ECL reagent (Thermo scientific, 32209). Quantitative densiometric analysis of the immunoblotted bands was performed using Image Labs software (BioRad Laboratories, V6.0.0) and data were normalized for each sample using stain-free technique.

Immunofluorescence staining

$CD4^+$ T cells were harvested after 72 h of anti-CD3 activation on cytoslides (Thermo scientific, 5991056) using a Shandon cytospin centrifuge (400 rpm for 4 min at RT). After drying, cells were fixed with 4% PFA in PBS for 15 min and washed 3 times, followed by membrane permeabilization with 0.1% Triton-X for 5 min. Un-specific binding was blocked with 5% bovine serum albumin and 10% donkey serum (Jackson ImmunoResearch, 017-000121) in 1X PBS for 60 min. Cells were then washed and incubated with primary antibodies diluted in blocking solution overnight at 4 °C followed by incubation with an AlexaFluor 488-conjugated AffiniPure Donkey Anti-Rabbit IgG secondary antibody (Jackson ImmunoResearch, 711-545-152, 1:500) for 1h at RT. Finally, cells were washed again and counterstained with DAPI for 5 min and slides were mounted in ProLongTM Gold antifade reagent (Invitrogen). Images were acquired using confocal microscopy (LSM700, Zeiss) with 63X objective. For statistics, ≥ 50 cells from 3 donors were quantified using ImageJ (NIH) software. Primary antibodies and concentrations included rabbit anti-insulin receptor, InsR (Invitrogen, PA5-29286, 1:800), rabbit anti-GABRR2 (Invitrogen, PA5-41008, 1:600), and rabbit anti-SGLT2 (ProteinTech, 24654-1-AP, 1:100).

***In vitro* Hexokinase activity assay**

Hexokinase activity was measured at RT indirectly as a readout of NADH production, a by-product of the reaction converting glucose-6-phosphate to 6 phosphogluconolacton by the enzyme glucose-6-phosphate dehydrogenase (GPDH). The cells were harvested, centrifugated and washed twice with PBS. Washed cells were resuspended in 1 ml assay buffer solution, on ice, included in the hexokinase enzymatic assay kit (Bio Vision, K789-100). After centrifugation at 4 °C for 5 min, the resulting supernatant was used as the final cell extract for the enzymatic assay.

Electrophysiological recordings

The electrophysiological recordings from the isolated $CD4^+$ T cells were done using the perforated whole-cell patch-clamp configuration. In order to keep the intracellular chloride concentration intact, gramicidin was used to obtain the perforated configuration. Gramicidin was diluted in DMSO at the stock concentration 2 mg/ml and the final concentration of the gramicidin in the pipette solution was 2.6 µg/ml. The pipette solution with the gramicidin was protected from light, kept cold and used within 2 hours after the preparation. After making the cell-attached configuration, the access resistance was monitored until characteristic slow and low-amplitude capacitance

212 transients were observed and the access resistance decreased from GΩ range to the
213 range of tens of MΩ. The extracellular solution (in mM) contained: 157 NaCl, 4.5 KCl,
214 0.5 $CaCl_2$, 1 $MgCl_2$, 5 HEPES and 5.6 or 16.7 glucose (pH 7.4, adjusted with NaOH).
215 The pipette solution consisted of (mM): 149 KCl, 2 $CaCl_2$, 1 $MgCl_2$, 1 NaCl, 10 HEPES,
216 5.6 or 16.7 glucose (pH 7.3 adjusted with KOH). The patch-clamp pipettes were made
217 from borosilicate glass and had a resistance of 12–14 MΩ when filled with the pipette
218 solution and immersed in the extracellular solution. Recordings were done using
219 Axopatch 200B amplifier, filtered at 2 kHz and digitized on-line at 10 kHz using an
220 analog-to-digital converter. To record the electrophysiological data Clampex 10.5
221 (Molecular Devices, San Jose, CA, USA) software was used. Currents were recorded
222 at +30 mV or by a ramp protocol, where the potential was changed from −80 to +80
223 mV in 1 s, the holding potential (Vh) was kept −40 mV. The single sweep duration was
224 20 s with a break between sweeps 5 s. After application of a drug, the chamber was
225 perfused 2-6 min with extracellular solution only before next application of a drug.
226 Currents in the absence of drugs or in the presence of picrotoxin were subtracted from
227 the test-drug current response.
228
229 **Live cell time-lapse real-time Ca^{2+} imaging**
230 Cells were loaded with a calcium indicator, 3 μM Fluo-8H AM (AAT Bioquest,
231 Pleasanton, CA) for 15 min at 37 °C and seeded on 5% 3-aminopropyltriethoxysilane-
232 coated coverslip for 15 min at 37 °C. Time lapse images were acquired by confocal
233 microscopy (LSM700, Zeiss) with 40X objective at an interval of 1-1.5 second per
234 image. Drugs were diluted in RPMI 1640 without phenol red and perfused at indicated
235 time and concentration by a peristaltic pump. After application of each drug, cells were
236 perfused with the extracellular solution (RPMI 1640) before next application. Area for
237 single cells was marked and absolute fluorescence intensity values (F) were extracted
238 using ZENBlue software. Relative intensity (F/Fmedian) for each cell was calculated
239 for every recorded image and plotted against time. Further, maximum relative intensity
240 of the cells under drug application time is considered as drug's response. Data is
241 represented for all cells and as box-whiskers plot.
242
243 **Metabolism Assay**
244 Isolated $CD4^+$ T cells were plated in a XF^e96 cell plates that were coated with Cell-
245 Tak (#354240, Corning, New York, USA) according to manufacturer's protocol. The
246 metabolic function of activated $CD4^+$ T cells cultured for 3 days *in vitro* was analyzed
247 by measuring the extracellular acidification rate (ECAR) using an XF^e96 extracellular
248 flux analyzer (Seahorse Bioscience). The cells were kept in XF media (Seahorse
249 Bioscience) supplemented with 5 mM glucose (Sigma Aldrich), and subjected to
250 glycolysis stress-test protocol using sequential injection of 25 mM glucose, 2 μM
251 oligomycin, and finally 15 mM 2-deoxyglucose (2DG). Measurements for each
252 experiment were conducted at least in triplicates and glycolysis, glycolytic capacity,
253 and glycolytic reserve calculated and values normalized to protein content [3, 4].
254
255 **Glucose uptake assay**
256 2x 10^6 activated $CD4^+$ T cells (72 h activation) with insulin treatment from 48 h after
257 activation were pelleted, resuspended in glucose-free RPMI-1640 media, incubated
258 for 10 min in the incubator at 37 °C, and washed once with the same media. Glucose-
259 free media (500 μl) containing 1μCi/ml [^{14}C] glucose (Perkin Elmer) were added to
260 cells in the absence or presence of phlorizin (100 μM) or empagliflozin (0.5 μM). Cells
261 were incubated for 40 min at 37 °C, pelleted by centrifugation at 300x g for 5 min and

washed three times in cold PBS. Cells were then lysed in RIPA buffer and ^{14}C content was measured with Gold XR scintillation fluid using a liquid scintillation counter (Perkin Elmer). The glucose uptake was calculated by normalizing counts to protein contents for each sample.

Statistical analysis

Statistical analysis was performed using GraphPad Prism 9 GraphPad Prism (GraphPad Software Inc., La Jolla, CA, Version 9.3.1). Normalized PEA data were assessed by two-tailed paired t-test followed by Benjamini-Hochberg's FDR (False Discovery Rate) method. The significance level is set to 10% FDR. Cellular metabolic activity, cytokine levels, mRNA, protein expression and ECAR of $CD4^+$ T cells in the presence of indicated drugs were normalized to controls (activated cells without drug treatment) from each donor and for each glucose concentration. Normalized data were analyzed by one-sample t-test when compared to controls. A comparison between paired groups was performed using repeated measures or mixed-model effects one-way ANOVA followed by Tukey or Fisher's LSD multiple comparisons tests. Unpaired multiple-group comparison was performed using ordinary one-way ANOVA followed by Tukey test. Changes in protein levels in MS data were analyzed using Quantitative, multi-dataset Pathway Analysis (ReactomeGSA, https://reactome.org/PathwayBrowser/#TOOL=AT)[5] and volcano plot was subsequently generated. Error bars in the bar graphs represent SEM unless otherwise specified and the statistical significance level was set to 0.05.

Additional references

1. Rofo, F. *et al.* Wide-Ranging Effects on the Brain Proteome in a Transgenic Mouse Model of Alzheimer's Disease Following Treatment with a Brain-Targeting Somatostatin Peptide. *ACS Chem Neurosci* **12**, 2529-2541 (2021).
2. Distler, U., Kuharev, J., Navarro, P. & Tenzer, S. Label-free quantification in ion mobility-enhanced data-independent acquisition proteomics. *Nat Protoc* **11**, 795-812 (2016).
3. Pelletier, M., Billingham, L.K., Ramaswamy, M. & Siegel, R.M. Extracellular flux analysis to monitor glycolytic rates and mitochondrial oxygen consumption. *Methods Enzymol* **542**, 125-149 (2014).
4. Traba, J., Miozzo, P., Akkaya, B., Pierce, S.K. & Akkaya, M. An Optimized Protocol to Analyze Glycolysis and Mitochondrial Respiration in Lymphocytes. *J Vis Exp* (2016).
5. ReactomeGSA - Efficient Multi-Omics Comparative Pathway AnalysisJohannes Griss, Guilherme Viteri, Konstantinos Sidiropoulos, Vy Nguyen, Antonio Fabregat, Henning Hermjakob. bioRxiv 2020.04.16.044958; doi: https://doi.org/10.1101/2020.04.16.044958